

Measurement of the $e^+e^- \rightarrow p\bar{p}\pi^0$ cross section at $\sqrt{s} = 2.1000 - 3.0800$ GeV

M. Ablikim¹, M. N. Achasov^{4,c}, P. Adlarson⁷⁵, O. Afedulidis³, X. C. Ai⁸⁰, R. Aliberti³⁵, A. Amoroso^{74A,74C}, Q. An^{71,58,a}, Y. Bai⁵⁷, O. Bakina³⁶, I. Balossino^{29A}, Y. Ban^{46,h}, H.-R. Bao⁶³, V. Batozskaya^{1,44}, K. Begzsuren³², N. Berger³⁵, M. Berlowski⁴⁴, M. Bertani^{28A}, D. Bettoni^{29A}, F. Bianchi^{74A,74C}, E. Bianco^{74A,74C}, A. Bortone^{74A,74C}, I. Boyko³⁶, R. A. Briere⁵, A. Brueggemann⁶⁸, H. Cai⁷⁶, X. Cai^{1,58}, A. Calcaterra^{28A}, G. F. Cao^{1,63}, N. Cao^{1,63}, S. A. Cetin^{62A}, J. F. Chang^{1,58}, G. R. Che⁴³, G. Chelkov^{36,b}, C. Chen⁴³, C. H. Chen⁹, Chao Chen⁵⁵, G. Chen¹, H. S. Chen^{1,63}, H. Y. Chen²⁰, M. L. Chen^{1,58,63}, S. J. Chen⁴², S. L. Chen⁴⁵, S. M. Chen⁶¹, T. Chen^{1,63}, X. R. Chen^{31,63}, X. T. Chen^{1,63}, Y. B. Chen^{1,58}, Y. Q. Chen³⁴, Z. J. Chen^{25,i}, Z. Y. Chen^{1,63}, S. K. Choi^{10A}, G. Cibinetto^{29A}, F. Cossio^{74C}, J. J. Cui⁵⁰, H. L. Dai^{1,58}, J. P. Dai⁷⁸, A. Dbeyssi¹⁸, R. E. de Boer³, D. Dedovich³⁶, C. Q. Deng⁷², Z. Y. Deng¹, A. Denig³⁵, I. Denysenko³⁶, M. Destefanis^{74A,74C}, F. De Mori^{74A,74C}, B. Ding^{66,1}, X. X. Ding^{46,h}, Y. Ding⁴⁰, Y. Ding³⁴, J. Dong^{1,58}, L. Y. Dong^{1,63}, M. Y. Dong^{1,58,63}, X. Dong⁷⁶, M. C. Du¹, S. X. Du⁸⁰, Y. Y. Duan⁵⁵, Z. H. Duan⁴², P. Egorov^{36,b}, Y. H. Fan⁴⁵, J. Fang^{1,58}, J. Fang⁵⁹, S. S. Fang^{1,63}, W. X. Fang¹, Y. Fang¹, Y. Q. Fang^{1,58}, R. Farinelli^{29A}, L. Fava^{74B,74C}, F. Feldbauer³, G. Felici^{28A}, C. Q. Feng^{71,58}, J. H. Feng⁵⁹, Y. T. Feng^{71,58}, M. Fritsch³, C. D. Fu¹, J. L. Fu⁶³, Y. W. Fu^{1,63}, H. Gao⁶³, X. B. Gao⁴¹, Y. N. Gao^{46,h}, Yang Gao^{71,58}, S. Garbolino^{74C}, I. Garzia^{29A,29B}, L. Ge⁸⁰, P. T. Ge⁷⁶, Z. W. Ge⁴², C. Geng⁵⁹, E. M. Gersabeck⁶⁷, A. Gilman⁶⁹, K. Goetzen¹³, L. Gong⁴⁰, W. X. Gong^{1,58}, W. Gradl³⁵, S. Gramigna^{29A,29B}, M. Greco^{74A,74C}, M. H. Gu^{1,58}, Y. T. Gu¹⁵, C. Y. Guan^{1,63}, A. Q. Guo^{31,63}, L. B. Guo⁴¹, M. J. Guo⁵⁰, R. P. Guo⁴⁹, Y. P. Guo^{12,g}, A. Guskov^{36,b}, J. Gutierrez²⁷, K. L. Han⁶³, T. T. Han¹, F. Hanisch³, X. Q. Hao¹⁹, F. A. Harris⁶⁵, K. K. He⁵⁵, K. L. He^{1,63}, F. H. Heinsius³, C. H. Heinz³⁵, Y. K. Heng^{1,58,63}, C. Herold⁶⁰, T. Holtmann³, P. C. Hong³⁴, G. Y. Hou^{1,63}, X. T. Hou^{1,63}, Y. R. Hou⁶³, Z. L. Hou¹, B. Y. Hu⁵⁹, H. M. Hu^{1,63}, J. F. Hu^{56,j}, S. L. Hu^{12,g}, T. Hu^{1,58,63}, Y. Hu¹, G. S. Huang^{71,58}, K. X. Huang⁵⁹, L. Q. Huang^{31,63}, X. T. Huang⁵⁰, Y. P. Huang¹, Y. S. Huang⁵⁹, T. Hussain⁷³, F. Hölzken³, N. Hüsken³⁵, N. in der Wiesche⁶⁸, J. Jackson²⁷, S. Janchiv³², J. H. Jeong^{10A}, Q. Ji¹, Q. P. Ji¹⁹, W. Ji^{1,63}, X. B. Ji^{1,63}, X. L. Ji^{1,58}, Y. Y. Ji⁵⁰, X. Q. Jia⁵⁰, Z. K. Jia^{71,58}, D. Jiang^{1,63}, H. B. Jiang⁷⁶, P. C. Jiang^{46,h}, S. S. Jiang³⁹, T. J. Jiang¹⁶, X. S. Jiang^{1,58,63}, Y. Jiang⁶³, J. B. Jiao⁵⁰, J. K. Jiao³⁴, Z. Jiao²³, S. Jin⁴², Y. Jin⁶⁶, M. Q. Jing^{1,63}, X. M. Jing⁶³, T. Johansson⁷⁵, S. Kabana³³, N. Kalantar-Nayestanaki⁶⁴, X. L. Kang⁹, X. S. Kang⁴⁰, M. Kavatsyuk⁶⁴, B. C. Ke⁸⁰, V. Khachatryan²⁷, A. Khoukaz⁶⁸, R. Kiuchi¹, O. B. Kolcu^{62A}, B. Kopf³, M. Kuessner³, X. Kui^{1,63}, N. Kumar²⁶, A. Kupsc^{44,75}, W. Kühn³⁷, J. J. Lane⁶⁷, P. Larin¹⁸, L. Lavezzi^{74A,74C}, T. T. Lei^{71,58}, Z. H. Lei^{71,58}, M. Lellmann³⁵, T. Lenz³⁵, C. Li⁴³, C. Li⁴⁷, C. H. Li³⁹, Cheng Li^{71,58}, D. M. Li⁸⁰, F. Li^{1,58}, G. Li¹, H. B. Li^{1,63}, H. J. Li¹⁹, H. N. Li^{56,j}, Hui Li⁴³, J. R. Li⁶¹, J. S. Li⁵⁹, K. Li¹, L. J. Li^{1,63}, L. K. Li¹, Lei Li⁴⁸, M. H. Li⁴³, P. R. Li^{38,k,l}, Q. M. Li^{1,63}, Q. X. Li⁵⁰, R. Li^{17,31}, S. X. Li¹², T. Li⁵⁰, W. D. Li^{1,63}, W. G. Li^{1,a}, X. Li^{1,63}, X. H. Li^{71,58}, X. L. Li⁵⁰, X. Y. Li^{1,63}, X. Z. Li⁵⁹, Y. G. Li^{46,h}, Z. J. Li⁵⁹, Z. Y. Li⁷⁸, C. Liang⁴², H. Liang^{71,58}, H. Liang^{1,63}, Y. F. Liang⁵⁴, Y. T. Liang^{31,63}, G. R. Liao¹⁴, L. Z. Liao⁵⁰, Y. P. Liao^{1,63}, J. Libby²⁶, A. Limphirat⁶⁰, C. C. Lin⁵⁵, D. X. Lin^{31,63}, T. Lin¹, B. J. Liu¹, B. X. Liu⁷⁶, C. Liu³⁴, C. X. Liu¹, F. Liu¹, F. H. Liu⁵³, Feng Liu⁶, G. M. Liu^{56,j}, H. Liu^{38,k,l}, H. B. Liu¹⁵, H. H. Liu¹, H. M. Liu^{1,63}, Huihui Liu²¹, J. B. Liu^{71,58}, J. Y. Liu^{1,63}, K. Liu^{38,k,l}, K. Y. Liu⁴⁰, Ke Liu²², L. Liu^{71,58}, L. C. Liu⁴³, Lu Liu⁴³, M. H. Liu^{12,g}, P. L. Liu¹, Q. Liu⁶³, S. B. Liu^{71,58}, T. Liu^{12,g}, W. K. Liu⁴³, W. M. Liu^{71,58}, X. Liu^{38,k,l}, X. Liu³⁹, Y. Liu^{38,k,l}, Y. Liu⁸⁰, Y. B. Liu⁴³, Z. A. Liu^{1,58,63}, Z. D. Liu⁹, Z. Q. Liu⁵⁰, X. C. Lou^{1,58,63}, F. X. Lu⁵⁹, H. J. Lu²³, J. G. Lu^{1,58}, X. L. Lu¹, Y. Lu⁷, Y. P. Lu^{1,58}, Z. H. Lu^{1,63}, C. L. Luo⁴¹, J. R. Luo⁵⁹, M. X. Luo⁷⁹, T. Luo^{12,g}, X. L. Luo^{1,58}, X. R. Lyu⁶³, Y. F. Lyu⁴³, F. C. Ma⁴⁰, H. Ma⁷⁸, H. L. Ma¹, J. L. Ma^{1,63}, L. L. Ma⁵⁰, M. M. Ma^{1,63}, Q. M. Ma¹, R. Q. Ma^{1,63}, T. Ma^{71,58}, X. T. Ma^{1,63}, X. Y. Ma^{1,58}, Y. Ma^{46,h}, Y. M. Ma³¹, F. E. Maas¹⁸, M. Maggiora^{74A,74C}, S. Malde⁶⁹, Y. J. Mao^{46,h}, Z. P. Mao¹, S. Marcello^{74A,74C}, Z. X. Meng⁶⁶, J. G. Messchendorp^{13,64}, G. Mezzadri^{29A}, H. Miao^{1,63}, T. J. Min⁴², R. E. Mitchell²⁷, X. H. Mo^{1,58,63}, B. Moses²⁷, N. Yu. Muchnoi^{4,c}, J. Muskalla³⁵, Y. Nefedov³⁶, F. Nerling^{18,e}, L. S. Nie²⁰, I. B. Nikolaev^{4,c}, Z. Ning^{1,58}, S. Nisar^{11,m}, Q. L. Niu^{38,k,l}, W. D. Niu⁵⁵, Y. Niu⁵⁰, S. L. Olsen⁶³, Q. Ouyang^{1,58,63}, S. Pacetti^{28B,28C}, X. Pan⁵⁵, Y. Pan⁵⁷, A. Pathak³⁴, P. Patteri^{28A}, Y. P. Pei^{71,58}, M. Pelizaes³, H. P. Peng^{71,58}, Y. Y. Peng^{38,k,l}, K. Peters^{13,e}, J. L. Ping⁴¹, R. G. Ping^{1,63}, S. Plura³⁵, V. Prasad³³, F. Z. Qi¹, H. Qi^{71,58}, H. R. Qi⁶¹, M. Qi⁴², T. Y. Qi^{12,g}, S. Qian^{1,58}, W. B. Qian⁶³, C. F. Qiao⁶³, X. K. Qiao⁸⁰, J. J. Qin⁷², L. Q. Qin¹⁴, L. Y. Qin^{71,58}, X. P. Qin^{12,g}, X. S. Qin⁵⁰, Z. H. Qin^{1,58}, J. F. Qiu¹, Z. H. Qu⁷², C. F. Redmer³⁵, K. J. Ren³⁹, A. Rivetti^{74C}, M. Rolo^{74C}, G. Rong^{1,63}, Ch. Rosner¹⁸, S. N. Ruan⁴³, N. Salone⁴⁴, A. Sarantsev^{36,d}, Y. Schelhaas³⁵, K. Schoenning⁷⁵, M. Scodreggio^{29A}, K. Y. Shan^{12,g}, W. Shan²⁴, X. Y. Shan^{71,58}, Z. J. Shang^{38,k,l}, J. F. Shanguan¹⁶, L. G. Shao^{1,63}, M. Shao^{71,58}, C. P. Shen^{12,g}, H. F. Shen^{1,8}, W. H. Shen⁶³, X. Y. Shen^{1,63}, B. A. Shi⁶³, H. Shi^{71,58}, H. C. Shi^{71,58}, J. L. Shi^{12,g}, J. Y. Shi¹, Q. Q. Shi⁵⁵, S. Y. Shi⁷², X. Shi^{1,58}, J. J. Song¹⁹, T. Z. Song⁵⁹, W. M. Song^{34,1}, Y. J. Song^{12,g}, Y. X. Song^{46,h,n}, S. Sosio^{74A,74C}, S. Spataro^{74A,74C}, F. Stieler³⁵, Y. J. Su⁶³, G. B. Sun⁷⁶, G. X. Sun¹, H. Sun⁶³, H. K. Sun¹, J. F. Sun¹⁹, K. Sun⁶¹, L. Sun⁷⁶, S. S. Sun^{1,63}, T. Sun^{51,f}, W. Y. Sun³⁴, Y. Sun⁹, Y. J. Sun^{71,58}, Y. Z. Sun¹, Z. Q. Sun^{1,63}, Z. T. Sun⁵⁰, C. J. Tang⁵⁴, G. Y. Tang¹, J. Tang⁵⁹, M. Tang^{71,58}, Y. A. Tang⁷⁶, L. Y. Tao⁷², Q. T. Tao^{25,i}, M. Tat⁶⁹, J. X. Teng^{71,58}, V. Thoren⁷⁵, W. H. Tian⁵⁹, Y. Tian^{31,63}, Z. F. Tian⁷⁶, I. Uman^{62B}, Y. Wan⁵⁵, S. J. Wang⁵⁰, B. Wang¹,

B. L. Wang⁶³, Bo Wang^{71,58}, D. Y. Wang^{46,h}, F. Wang⁷², H. J. Wang^{38,k,l}, J. J. Wang⁷⁶, J. P. Wang⁵⁰, K. Wang^{1,58},
 L. L. Wang¹, M. Wang⁵⁰, N. Y. Wang⁶³, S. Wang^{12,g}, S. Wang^{38,k,l}, T. Wang^{12,g}, T. J. Wang⁴³, W. Wang⁵⁹, W.
 Wang⁷², W. P. Wang^{35,71,o}, X. Wang^{46,h}, X. F. Wang^{38,k,l}, X. J. Wang³⁹, X. L. Wang^{12,g}, X. N. Wang¹, Y. Wang⁶¹,
 Y. D. Wang⁴⁵, Y. F. Wang^{1,58,63}, Y. L. Wang¹⁹, Y. N. Wang⁴⁵, Y. Q. Wang¹, Yaqian Wang¹⁷, Yi Wang⁶¹, Z. Wang^{1,58},
 Z. L. Wang⁷², Z. Y. Wang^{1,63}, Ziyi Wang⁶³, D. H. Wei¹⁴, F. Weidner⁶⁸, S. P. Wen¹, Y. R. Wen³⁹, U. Wiedner³,
 G. Wilkinson⁶⁹, M. Wolke⁷⁵, L. Wollenberg³, C. Wu³⁹, J. F. Wu^{1,8}, L. H. Wu¹, L. J. Wu^{1,63}, X. Wu^{12,g}, X. H. Wu³⁴,
 Y. Wu^{71,58}, Y. H. Wu⁵⁵, Y. J. Wu³¹, Z. Wu^{1,58}, L. Xia^{71,58}, X. M. Xian³⁹, B. H. Xiang^{1,63}, T. Xiang^{46,h}, D. Xiao^{38,k,l},
 G. Y. Xiao⁴², S. Y. Xiao¹, Y. L. Xiao^{12,g}, Z. J. Xiao⁴¹, C. Xie⁴², X. H. Xie^{46,h}, Y. Xie⁵⁰, Y. G. Xie^{1,58}, Y. H. Xie⁶,
 Z. P. Xie^{71,58}, T. Y. Xing^{1,63}, C. F. Xu^{1,63}, C. J. Xu⁵⁹, G. F. Xu¹, H. Y. Xu^{66,2,p}, M. Xu^{71,58}, Q. J. Xu¹⁶, Q. N. Xu³⁰,
 W. Xu¹, W. L. Xu⁶⁶, X. P. Xu⁵⁵, Y. C. Xu⁷⁷, Z. P. Xu⁴², Z. S. Xu⁶³, F. Yan^{12,g}, L. Yan^{12,g}, W. B. Yan^{71,58}, W. C. Yan⁸⁰,
 X. Q. Yan¹, H. J. Yang^{51,f}, H. L. Yang³⁴, H. X. Yang¹, T. Yang¹, Y. Yang^{12,g}, Y. F. Yang^{1,63}, Y. F. Yang⁴³,
 Y. X. Yang^{1,63}, Z. W. Yang^{38,k,l}, Z. P. Yao⁵⁰, M. Ye^{1,58}, M. H. Ye⁸, J. H. Yin¹, Z. Y. You⁵⁹, B. X. Yu^{1,58,63}, C. X. Yu⁴³,
 G. Yu^{1,63}, J. S. Yu^{25,i}, T. Yu⁷², X. D. Yu^{46,h}, Y. C. Yu⁸⁰, C. Z. Yuan^{1,63}, J. Yuan³⁴, J. Yuan⁴⁵, L. Yuan², S. C. Yuan^{1,63},
 Y. Yuan^{1,63}, Z. Y. Yuan⁵⁹, C. X. Yue³⁹, A. A. Zafar⁷³, F. R. Zeng⁵⁰, S. H. Zeng⁷², X. Zeng^{12,g}, Y. Zeng^{25,i},
 Y. J. Zeng^{1,63}, Y. J. Zeng⁵⁹, X. Y. Zhai³⁴, Y. C. Zhai⁵⁰, Y. H. Zhan⁵⁹, A. Q. Zhang^{1,63}, B. L. Zhang^{1,63}, B. X. Zhang¹,
 D. H. Zhang⁴³, G. Y. Zhang¹⁹, H. Zhang⁸⁰, H. Zhang^{71,58}, H. C. Zhang^{1,58,63}, H. H. Zhang³⁴, H. H. Zhang⁵⁹,
 H. Q. Zhang^{1,58,63}, H. R. Zhang^{71,58}, H. Y. Zhang^{1,58}, J. Zhang⁸⁰, J. Zhang⁵⁹, J. J. Zhang⁵², J. L. Zhang²⁰,
 J. Q. Zhang⁴¹, J. S. Zhang^{12,g}, J. W. Zhang^{1,58,63}, J. X. Zhang^{38,k,l}, J. Y. Zhang¹, J. Z. Zhang^{1,63}, Jianyu Zhang⁶³,
 L. M. Zhang⁶¹, Lei Zhang⁴², P. Zhang^{1,63}, Q. Y. Zhang³⁴, R. Y. Zhang^{38,k,l}, S. H. Zhang^{1,63}, Shulei Zhang^{25,i},
 X. D. Zhang⁴⁵, X. M. Zhang¹, X. Y. Zhang⁵⁰, Y. Zhang⁷², Y. Zhang¹, Y. T. Zhang⁸⁰, Y. H. Zhang^{1,58}, Y. M. Zhang³⁹,
 Yan Zhang^{71,58}, Z. D. Zhang¹, Z. H. Zhang¹, Z. L. Zhang³⁴, Z. Y. Zhang⁷⁶, Z. Y. Zhang⁴³, Z. Z. Zhang⁴⁵, G. Zhao¹,
 J. Y. Zhao^{1,63}, J. Z. Zhao^{1,58}, L. Zhao¹, Lei Zhao^{71,58}, M. G. Zhao⁴³, N. Zhao⁷⁸, R. P. Zhao⁶³, S. J. Zhao⁸⁰,
 Y. B. Zhao^{1,58}, Y. X. Zhao^{31,63}, Z. G. Zhao^{71,58}, A. Zhemchugov^{36,b}, B. Zheng⁷², B. M. Zheng³⁴, J. P. Zheng^{1,58},
 W. J. Zheng^{1,63}, Y. H. Zheng⁶³, B. Zhong⁴¹, X. Zhong⁵⁹, H. Zhou⁵⁰, J. Y. Zhou³⁴, L. P. Zhou^{1,63}, S. Zhou⁶, X. Zhou⁷⁶,
 X. K. Zhou⁶, X. R. Zhou^{71,58}, X. Y. Zhou³⁹, Y. Z. Zhou^{12,g}, J. Zhu⁴³, K. Zhu¹, K. J. Zhu^{1,58,63}, K. S. Zhu^{12,g}, L. Zhu³⁴,
 L. X. Zhu⁶³, S. H. Zhu⁷⁰, S. Q. Zhu⁴², T. J. Zhu^{12,g}, W. D. Zhu⁴¹, Y. C. Zhu^{71,58}, Z. A. Zhu^{1,63}, J. H. Zou¹, J. Zu^{71,58}

(BESIII Collaboration)

¹ *Institute of High Energy Physics, Beijing 100049, People's Republic of China*

² *Beihang University, Beijing 100191, People's Republic of China*

³ *Bochum Ruhr-University, D-44780 Bochum, Germany*

⁴ *Budker Institute of Nuclear Physics SB RAS (BINP), Novosibirsk 630090, Russia*

⁵ *Carnegie Mellon University, Pittsburgh, Pennsylvania 15213, USA*

⁶ *Central China Normal University, Wuhan 430079, People's Republic of China*

⁷ *Central South University, Changsha 410083, People's Republic of China*

⁸ *China Center of Advanced Science and Technology, Beijing 100190, People's Republic of China*

⁹ *China University of Geosciences, Wuhan 430074, People's Republic of China*

¹⁰ *Chung-Ang University, Seoul, 06974, Republic of Korea*

¹¹ *COMSATS University Islamabad, Lahore Campus, Defence Road, Off Raiwind Road, 54000 Lahore, Pakistan*

¹² *Fudan University, Shanghai 200433, People's Republic of China*

¹³ *GSI Helmholtzcentre for Heavy Ion Research GmbH, D-64291 Darmstadt, Germany*

¹⁴ *Guangxi Normal University, Guilin 541004, People's Republic of China*

¹⁵ *Guangxi University, Nanning 530004, People's Republic of China*

¹⁶ *Hangzhou Normal University, Hangzhou 310036, People's Republic of China*

¹⁷ *Hebei University, Baoding 071002, People's Republic of China*

¹⁸ *Helmholtz Institute Mainz, Staudinger Weg 18, D-55099 Mainz, Germany*

¹⁹ *Henan Normal University, Xinxiang 453007, People's Republic of China*

²⁰ *Henan University, Kaifeng 475004, People's Republic of China*

²¹ *Henan University of Science and Technology, Luoyang 471003, People's Republic of China*

²² *Henan University of Technology, Zhengzhou 450001, People's Republic of China*

²³ *Huangshan College, Huangshan 245000, People's Republic of China*

²⁴ *Hunan Normal University, Changsha 410081, People's Republic of China*

²⁵ *Hunan University, Changsha 410082, People's Republic of China*

²⁶ *Indian Institute of Technology Madras, Chennai 600036, India*

²⁷ *Indiana University, Bloomington, Indiana 47405, USA*

²⁸ *INFN Laboratori Nazionali di Frascati, (A)INFN Laboratori Nazionali di Frascati, I-00044, Frascati, Italy;*

- (B)INFN Sezione di Perugia, I-06100, Perugia, Italy; (C)University of Perugia, I-06100, Perugia, Italy
- ²⁹ INFN Sezione di Ferrara, (A)INFN Sezione di Ferrara, I-44122, Ferrara, Italy; (B)University of Ferrara, I-44122, Ferrara, Italy
- ³⁰ Inner Mongolia University, Hohhot 010021, People's Republic of China
- ³¹ Institute of Modern Physics, Lanzhou 730000, People's Republic of China
- ³² Institute of Physics and Technology, Peace Avenue 54B, Ulaanbaatar 13330, Mongolia
- ³³ Instituto de Alta Investigación, Universidad de Tarapacá, Casilla 7D, Arica 1000000, Chile
- ³⁴ Jilin University, Changchun 130012, People's Republic of China
- ³⁵ Johannes Gutenberg University of Mainz, Johann-Joachim-Becher-Weg 45, D-55099 Mainz, Germany
- ³⁶ Joint Institute for Nuclear Research, 141980 Dubna, Moscow region, Russia
- ³⁷ Justus-Liebig-Universitaet Giessen, II. Physikalisches Institut, Heinrich-Buff-Ring 16, D-35392 Giessen, Germany
- ³⁸ Lanzhou University, Lanzhou 730000, People's Republic of China
- ³⁹ Liaoning Normal University, Dalian 116029, People's Republic of China
- ⁴⁰ Liaoning University, Shenyang 110036, People's Republic of China
- ⁴¹ Nanjing Normal University, Nanjing 210023, People's Republic of China
- ⁴² Nanjing University, Nanjing 210093, People's Republic of China
- ⁴³ Nankai University, Tianjin 300071, People's Republic of China
- ⁴⁴ National Centre for Nuclear Research, Warsaw 02-093, Poland
- ⁴⁵ North China Electric Power University, Beijing 102206, People's Republic of China
- ⁴⁶ Peking University, Beijing 100871, People's Republic of China
- ⁴⁷ Qufu Normal University, Qufu 273165, People's Republic of China
- ⁴⁸ Renmin University of China, Beijing 100872, People's Republic of China
- ⁴⁹ Shandong Normal University, Jinan 250014, People's Republic of China
- ⁵⁰ Shandong University, Jinan 250100, People's Republic of China
- ⁵¹ Shanghai Jiao Tong University, Shanghai 200240, People's Republic of China
- ⁵² Shanxi Normal University, Linfen 041004, People's Republic of China
- ⁵³ Shanxi University, Taiyuan 030006, People's Republic of China
- ⁵⁴ Sichuan University, Chengdu 610064, People's Republic of China
- ⁵⁵ Soochow University, Suzhou 215006, People's Republic of China
- ⁵⁶ South China Normal University, Guangzhou 510006, People's Republic of China
- ⁵⁷ Southeast University, Nanjing 211100, People's Republic of China
- ⁵⁸ State Key Laboratory of Particle Detection and Electronics, Beijing 100049, Hefei 230026, People's Republic of China
- ⁵⁹ Sun Yat-Sen University, Guangzhou 510275, People's Republic of China
- ⁶⁰ Suranaree University of Technology, University Avenue 111, Nakhon Ratchasima 30000, Thailand
- ⁶¹ Tsinghua University, Beijing 100084, People's Republic of China
- ⁶² Turkish Accelerator Center Particle Factory Group, (A)Istinye University, 34010, Istanbul, Turkey; (B)Near East University, Nicosia, North Cyprus, 99138, Mersin 10, Turkey
- ⁶³ University of Chinese Academy of Sciences, Beijing 100049, People's Republic of China
- ⁶⁴ University of Groningen, NL-9747 AA Groningen, The Netherlands
- ⁶⁵ University of Hawaii, Honolulu, Hawaii 96822, USA
- ⁶⁶ University of Jinan, Jinan 250022, People's Republic of China
- ⁶⁷ University of Manchester, Oxford Road, Manchester, M13 9PL, United Kingdom
- ⁶⁸ University of Muenster, Wilhelm-Klemm-Strasse 9, 48149 Muenster, Germany
- ⁶⁹ University of Oxford, Keble Road, Oxford OX13RH, United Kingdom
- ⁷⁰ University of Science and Technology Liaoning, Anshan 114051, People's Republic of China
- ⁷¹ University of Science and Technology of China, Hefei 230026, People's Republic of China
- ⁷² University of South China, Hengyang 421001, People's Republic of China
- ⁷³ University of the Punjab, Lahore-54590, Pakistan
- ⁷⁴ University of Turin and INFN, (A)University of Turin, I-10125, Turin, Italy; (B)University of Eastern Piedmont, I-15121, Alessandria, Italy; (C)INFN, I-10125, Turin, Italy
- ⁷⁵ Uppsala University, Box 516, SE-75120 Uppsala, Sweden
- ⁷⁶ Wuhan University, Wuhan 430072, People's Republic of China
- ⁷⁷ Yantai University, Yantai 264005, People's Republic of China
- ⁷⁸ Yunnan University, Kunming 650500, People's Republic of China
- ⁷⁹ Zhejiang University, Hangzhou 310027, People's Republic of China
- ⁸⁰ Zhengzhou University, Zhengzhou 450001, People's Republic of China

^a Deceased

^b Also at the Moscow Institute of Physics and Technology, Moscow 141700, Russia

^c Also at the Novosibirsk State University, Novosibirsk, 630090, Russia

^d Also at the NRC "Kurchatov Institute", PNPI, 188300, Gatchina, Russia

^e Also at Goethe University Frankfurt, 60323 Frankfurt am Main, Germany

^f Also at Key Laboratory for Particle Physics, Astrophysics and Cosmology, Ministry of Education; Shanghai Key Laboratory for Particle Physics and Cosmology; Institute of Nuclear and Particle Physics, Shanghai 200240, People's Republic of China

^g Also at Key Laboratory of Nuclear Physics and Ion-beam Application (MOE) and Institute of Modern Physics, Fudan University, Shanghai 200443, People's Republic of China

^h Also at State Key Laboratory of Nuclear Physics and Technology, Peking University, Beijing 100871, People's Republic of China

ⁱ Also at School of Physics and Electronics, Hunan University, Changsha 410082, China

^j Also at Guangdong Provincial Key Laboratory of Nuclear Science, Institute of Quantum Matter, South China Normal University, Guangzhou 510006, China

^k Also at MOE Frontiers Science Center for Rare Isotopes, Lanzhou University, Lanzhou 730000, People's Republic of China

^l Also at Lanzhou Center for Theoretical Physics, Lanzhou University, Lanzhou 730000, People's Republic of China

^m Also at the Department of Mathematical Sciences, IBA, Karachi 75270, Pakistan

ⁿ Also at Ecole Polytechnique Federale de Lausanne (EPFL), CH-1015 Lausanne, Switzerland

^o Also at Helmholtz Institute Mainz, Staudinger Weg 18, D-55099 Mainz, Germany

^p Also at School of Physics, Beihang University, Beijing 100191, China

(Dated: May 13, 2024)

The process $e^+e^- \rightarrow p\bar{p}\pi^0$ is studied at 20 center-of-mass energies ranging from 2.1000 to 3.0800 GeV using 636.8 pb⁻¹ of data collected with the BESIII detector operating at the BEPCII collider. The Born cross sections for $e^+e^- \rightarrow p\bar{p}\pi^0$ are measured with high precision. Since the lowest center-of-mass energy, 2.1000 GeV, is less than 90 MeV above the $p\bar{p}\pi^0$ energy threshold, we can probe the threshold behavior for this reaction. However, no anomalous threshold enhancement is found in the cross sections for $e^+e^- \rightarrow p\bar{p}\pi^0$.

I. INTRODUCTION

Studies of threshold enhancements in the pair production of ground-state baryons in the spin- $\frac{1}{2}$ $SU(3)$ octet provide important information about the interactions and fundamental structure of particles. Significant threshold enhancements have previously been observed in the cross sections for the processes $e^+e^- \rightarrow p\bar{p}$ [1–5], $e^+e^- \rightarrow \Lambda_c\bar{\Lambda}_c$ [6, 7], $e^+e^- \rightarrow \Lambda\bar{\Lambda}$ [8, 9], etc. A common feature in the measured cross sections for many of these processes is a plateau starting from the baryon pair production threshold [10]. For asymmetric baryon pair, a non-zero Born cross section for the process $e^+e^- \rightarrow \Lambda\bar{\Sigma}^0 + c.c.$ at center-of-mass (c.m.) energy (\sqrt{s}) of 2.3094 GeV, which is about 1 MeV above the production threshold, is observed with a statistical significance of more than five standard deviations [11]. Within the process $e^+e^- \rightarrow p\bar{p}\pi^0$, the subprocess $e^+e^- \rightarrow \bar{p}N^* + c.c.$ or $e^+e^- \rightarrow \bar{p}\Delta^* + c.c.$, where N^* and Δ^* couple to $p\pi^0$, could potentially show a similar behavior.

The Born cross sections of $e^+e^- \rightarrow p\bar{p}\pi^0$ have previously been investigated in the charmonium region at BESIII. For example, around the $\psi(3770)$ resonance the e^+e^- cross sections have been measured and the Born cross section of $\psi(3770) \rightarrow p\bar{p}\pi^0$ has been extracted considering interference between resonant and continuum production amplitudes [12]. Also, at \sqrt{s} ranging from 4.008 to 4.600 GeV this process has been studied to explore the properties of charmonium states [13]. However, measure-

ments of the Born cross sections at lower \sqrt{s} , especially near the $p\bar{p}\pi^0$ production energy threshold, remain insufficient. Accurately characterizing the cross sections for $e^+e^- \rightarrow p\bar{p}\pi^0$ in the lower energy domain poses significant challenges and tests for perturbative QCD, especially near the threshold. In addition, these Born cross sections can be used to estimate the cross sections for $p\bar{p} \rightarrow e^+e^-\pi^0$. These in turn can be used to measure the proton form factor in the unphysical region [14], which is a goal for the future anti-Proton ANnihilations DArmstadt (\bar{P} ANDA) experiment at the Facility of Anti-proton and Ion Research (FAIR) in Germany [15].

In this paper, we report measurements of the Born cross sections for the process $e^+e^- \rightarrow p\bar{p}\pi^0$, obtained by analyzing e^+e^- collision data collected with the BESIII detector at \sqrt{s} ranging from 2.1000 to 3.0800 GeV with a total integrated luminosity of 636.8 pb⁻¹.

II. THE BESIII DETECTOR AND DATA SAMPLES

The BESIII detector [16] records symmetric e^+e^- collisions provided by the BEPCII storage ring [17] in the c.m. energy range from 2.00 up to 4.95 GeV, with a peak luminosity of 1.1×10^{33} cm⁻²s⁻¹ achieved at $\sqrt{s} = 3.773$ GeV. The cylindrical core of the BESIII detector covers 93% of the full solid angle and consists of a helium-based multilayer drift chamber (MDC), a plastic scintillator time-of-flight system (TOF), and a CsI(Tl) electromag-

netic calorimeter (EMC), which are all enclosed in a superconducting solenoidal magnet providing a 1.0 T magnetic field [18]. The solenoid is supported by an octagonal flux-return yoke with resistive plate counter muon identification modules interleaved with steel. The charged particle momentum resolution at 1 GeV/c is 0.5%, and the dE/dx resolution is 6% for electrons from Bhabha scattering. The EMC measures photon energies with a resolution of 2.5% (5%) at 1 GeV in the barrel (end cap) region. The time resolution in the TOF barrel region is 68 ps, while that in the end cap region is 110 ps.

Simulated data samples produced with a GEANT4-based [19] Monte Carlo (MC) package, which includes the geometric description of the BESIII detector and the detector response, are used to determine detection efficiencies and to estimate backgrounds. To estimate the detection efficiency, signal MC events are generated by CONEXC [20] using an amplitude model with all parameters fixed to the results obtained from the Feynman Diagram Calculation-Partial Wave Analysis (FDC-PWA) package [21]. Inclusive hadronic MC samples are generated with a hybrid generator that integrates CONEXC [20], PHOKHARA [22] and LUARLW [23].

III. EVENT SELECTION

Candidate $e^+e^- \rightarrow p\bar{p}\pi^0$ events are reconstructed using the final state $p\bar{p}\gamma\gamma$. Charged tracks detected in the MDC are required to be within a polar angle (θ) range of $|\cos\theta| < 0.93$, where θ is defined with respect to the z axis, which is the symmetry axis of the MDC. The distance of closest approach to the interaction point (IP) must be less than 10 cm along the z axis (denoted as $|V_z|$) and less than 1 cm in the transverse plane (denoted as $|V_{xy}|$). For each signal candidate, one or two charged tracks are required, in the case of partial or full reconstruction, respectively, as explained in the next subsections. Particle identification (PID) for charged tracks combines measurements of the energy deposited in the MDC (dE/dx) and the flight time in the TOF to calculate the probabilities for the pion, kaon, and proton hypotheses. In particular, for partial reconstruction the probability for the electron hypothesis is also considered. The particle type with the highest probability is assigned to the charged track. Charged tracks are constrained to originate from a common vertex.

Photon candidates are identified using showers in the EMC. The deposited energy of each shower must be more than 25 MeV in the barrel region ($|\cos\theta| < 0.80$) and more than 50 MeV in the end cap region ($0.86 < |\cos\theta| < 0.92$). To suppress electronic noise and showers unrelated to the event, the difference between the EMC time and the event start time is required to be within $[0, 700]$ ns.

At low center-of-mass energies near the $p\bar{p}\pi^0$ threshold, the detection efficiency decreases due to low momenta of the pions and (anti-)protons, which are less than 0.2 GeV/c and 0.35 GeV/c at $\sqrt{s} = 2.1250$ GeV, respectively. At higher \sqrt{s} , from 2.3094 to 3.0800 GeV, the increased momenta of the pions and (anti-)protons improve the detection efficiency. Therefore, we use a partial reconstruction

technique at \sqrt{s} from 2.1000 to 2.2324 GeV, and employ full reconstruction from 2.3094 to 3.0800 GeV.

A. Partial Reconstruction

Partial reconstruction of signal candidates is categorized into two modes. In Mode I, events with a missing π^0 are reconstructed; while in Mode II, events are missing a proton (p_{miss}). In Mode II, the π^0 is reconstructed by two photons. Both modes are used to increase the efficiency, and they are mutually exclusive with no overlap.

In Mode I, one proton, one anti-proton, and no photons are required. In order to suppress cosmic ray and beam backgrounds, the angle between the two charged tracks ($\theta_{p\bar{p}}$) is required to be less than 173° . A requirement on the recoil polar angle of the $p\bar{p}$ system ($\cos\theta_{p\bar{p}}^{\text{recoil}}$), $|\cos\theta_{p\bar{p}}^{\text{recoil}}| \leq 0.96$, is used to suppress the dominant background process, $e^+e^- \rightarrow p\bar{p}$ produced along with initial state radiation (ISR). The signal yield is obtained by performing an unbinned maximum-likelihood fit to the recoil mass spectrum of the $p\bar{p}$ pair ($M_{p\bar{p}}^{\text{recoil}}$). The signal is modeled using the MC-simulated shape convolved with a Gaussian function to account for potential differences in calibration and resolution between data and MC simulation. The background is modeled using a Landau function [24]. The fit result for data taken at $\sqrt{s} = 2.1250$ GeV is shown in Fig. 1. An identical set of event selection criteria and the same fit procedure are applied for all data below $\sqrt{s} = 2.2324$ GeV. The fit results ($N_{\text{Signal}}^{\text{Mode I}}$) are summarized in Table I.

In Mode II, at least two photons, one anti-proton, and no protons are required. To exclude showers that originate from the anti-proton, the angle subtended by the EMC shower and the position of the closest anti-proton track at the EMC must be greater than 30° as measured from the IP ($\theta_{\gamma\bar{p}}$). In order to further suppress background, a one-constraint (1C) kinematic fit imposing energy-momentum conservation is performed under the hypothesis of $p_{\text{miss}}\bar{p}\gamma\gamma$, treating the proton as a missing particle. The combination with the minimum $\chi_{1\text{C}}^2$ is retained, where $\chi_{1\text{C}}^2$ is the chi-square value of the 1C kinematic fit. The requirement on $\chi_{1\text{C}}^2$ has been optimized, and a cut of $\chi_{1\text{C}}^2 \leq 60$ has been imposed. The number of signal events is extracted by a simultaneous fit to the reconstructed π^0 mass spectrum, $M(\gamma\gamma)$, at each energy point below $\sqrt{s} = 2.2324$ GeV. An example is shown in Fig. 1 for data at $\sqrt{s} = 2.1250$ GeV. The signal is modeled using the MC-simulated shape convolved with a Gaussian function. The parameters of the smeared Gaussian function are considered as common parameters and are shared for different data samples at \sqrt{s} from 2.1000 to 2.2324 GeV. The background is described by a linear function. The fit results ($N_{\text{Signal}}^{\text{Mode II}}$) are listed in Table I, the last column of which lists the combined results (N_{Signal}). The combined results are calculated by $N_{\text{Signal}}^{\text{Mode I}} + N_{\text{Signal}}^{\text{Mode II}}$, with uncertainties determined through error propagation.

TABLE I. The signal yields of Mode I ($N_{\text{Signal}}^{\text{Mode I}}$) and Mode II ($N_{\text{Signal}}^{\text{Mode II}}$) and the combined results (N_{Signal}) at \sqrt{s} from 2.1000 to 2.2324 GeV. The uncertainties are statistical only.

\sqrt{s} (GeV)	$N_{\text{Signal}}^{\text{Mode I}}$	$N_{\text{Signal}}^{\text{Mode II}}$	N_{Signal}
2.1000	$5.5^{+3.6}_{-2.9}$	$2.4^{+2.3}_{-1.6}$	$7.9^{+4.3}_{-3.3}$
2.1250	189.0 ± 15.8	105.7 ± 11.9	294.7 ± 19.8
2.1500	18.8 ± 4.6	$4.4^{+3.4}_{-2.6}$	$23.2^{+5.7}_{-5.3}$
2.1750	78.9 ± 10.3	22.0 ± 5.5	100.9 ± 11.7
2.2200	163.5 ± 13.7	35.3 ± 6.9	198.8 ± 15.3
2.2324	175.2 ± 14.3	27.3 ± 6.1	202.5 ± 15.5

B. Full Reconstruction

At c.m. energies above 2.3094 GeV, full reconstruction is used, where each signal candidate is reconstructed by two charged tracks and a minimum of two photons. One proton and one anti-proton with zero net charge are required. The angle subtended by the EMC shower and the position of the closest charged proton track at the EMC must be greater than 10° as measured from the IP. The corresponding requirement for the anti-proton differs from the one adopted for Mode II and has been optimized at 20° instead of 30° . A four-constraint (4C) kinematic fit, which ensures energy-momentum conservation for a $p\bar{p}\gamma\gamma$ final state, is applied to the accepted candidates. In events containing more than two photon candidates, the combination with the minimum chi-square of the 4C kinematic fit (χ_{4C}^2) is selected. Candidate events with $\chi_{4C}^2 \leq 100$ are kept for further analysis.

After all the above selection criteria are applied, the signal yield for the $e^+e^- \rightarrow p\bar{p}\pi^0$ process is obtained by fitting the $M(\gamma\gamma)$ spectrum. The signal shape is derived from the signal MC sample and is convolved with a Gaussian function, where the Gaussian parameters are float at different energy points from 2.3094 to 3.0800 GeV. A linear function is used to describe the background. Figure 1 illustrates the fit result at $\sqrt{s} = 2.6444$ GeV as an example and fit results for all energy points are summarized in Table II.

IV. BORN CROSS SECTIONS OF $e^+e^- \rightarrow p\bar{p}\pi^0$

The Born cross section (σ^B) for $e^+e^- \rightarrow p\bar{p}\pi^0$ at each energy point is determined by

$$\sigma^B(\sqrt{s}) = \frac{N_{\text{Signal}}}{\mathcal{L} \cdot \epsilon \cdot \mathcal{B}(\pi^0 \rightarrow \gamma\gamma) \cdot (1 + \delta) \cdot \frac{1}{|1 - \Pi|^2}}, \quad (1)$$

where N_{Signal} is the number of signal events, \mathcal{L} is the integrated luminosity of data, $(1 + \delta)$ is the ISR correction factor and $\frac{1}{|1 - \Pi|^2}$ is the vacuum polarization (VP) factor. For the full reconstruction, the π^0 only decays to $\gamma\gamma$ in the signal MC simulation, so the Born cross sections are corrected by the branching fraction of $\pi^0 \rightarrow \gamma\gamma$ ($\mathcal{B}(\pi^0 \rightarrow \gamma\gamma)$) given by the Particle Data Group (PDG) [25]. In both Mode I and Mode II, $\mathcal{B}(\pi^0 \rightarrow \gamma\gamma)$ has been considered in the MC simulation. Additionally, ϵ represents the detection efficiency obtained by analyzing the signal MC events.

The signal MC events are generated using an amplitude model. The amplitudes of the quasi-two-body decays in the sequential decays are constructed using covariant tensor amplitudes [21]. At $\sqrt{s} = 2.6444$ GeV the process $e^+e^- \rightarrow p\bar{p}\pi^0$ is found to be well described by the following four subprocesses: $e^+e^- \rightarrow \rho(1900)\pi^0$, $e^+e^- \rightarrow N(1520)p$, $e^+e^- \rightarrow N(1650)p$ and $e^+e^- \rightarrow \Delta(1232)p$, where the charge conjugation processes are also considered. The intermediate states are parameterized by a relativistic Breit-Wigner formula, with mass and width fixed to the values from the PDG [25]. The complex coupling constants of the amplitudes are determined by an unbinned maximum-likelihood fit. The selection of components is evaluated at the energy points with the relatively high statistics, *i.e.*, at 2.1250, 2.3960, 2.6444 combined together with 2.6464, 2.9000 and 3.0800 GeV. These solutions are set as reference for other data sets at nearby energy points, and the data sets at 2.1000, 2.1500, and 2.1750 GeV use the fit results obtained at 2.1250 GeV due to their limited statistics. The solution used at each energy point is summarized in Table III. At all c.m. energies, the weighted signal MC simulation is in reasonable agreement with data, which can be seen at $\sqrt{s} = 2.6444$ GeV in Fig. 2 as an example.

The ISR correction factor and the detection efficiency are estimated based on signal MC samples, and then weighted by an iterative MC weighting method [26], with the iterative procedure repeated until the measured Born cross sections converge. The corresponding Born cross sections are summarized in Table II and shown in Fig. 3.

V. SYSTEMATIC UNCERTAINTY

Several sources of systematic uncertainties are considered in the determination of the Born cross sections. The uncertainty of the luminosity measurement is less than 0.9% [27]. The uncertainties associated with the tracking and PID efficiency for (anti-)protons are studied by a control sample of $J/\psi \rightarrow p\bar{p}\pi^+\pi^-$ and are obtained by averaging the uncertainties weighted by signal events in each transverse momentum bin. The uncertainty due to the photon reconstruction is 1.0%, leading to a total uncertainty of 2.0% for the two photons for Mode II [28]. Both uncertainties due to the $\theta_{\gamma\bar{p}} \geq 30^\circ$ and $\theta_{\gamma p} \geq 20^\circ$ requirements are studied by a control sample of $J/\psi \rightarrow p\bar{p}\pi^0$, which are set to be 0.8% and 0.3% per photon for Mode II and full reconstruction, respectively. The uncertainty of the branching fraction of $\pi^0 \rightarrow \gamma\gamma$ quoted from the PDG [25] is 0.03% for full reconstruction, which is neglected.

In Mode I, the uncertainties due to both $\theta_{p\bar{p}} \leq 173^\circ$ and $|\cos\theta_{\pi^0}| \leq 0.96$ requirements are assigned as 0.3% and 0.4% based on a study of the $J/\psi \rightarrow p\bar{p}\pi^0$ control sample. In Mode II, the uncertainty from the kinematic fit is also studied with the $J/\psi \rightarrow p\bar{p}\pi^0$ control sample. The difference in selection efficiency before and after the kinematic fit for data and MC simulation, 0.1%, is taken as the systematic uncertainty. In full reconstruction, the uncertainty due to the π^0 reconstruction, including the photon selection efficiency, is estimated to be 2.5%, based on an analysis of the $J/\psi \rightarrow p\bar{p}\pi^0$ control sample.

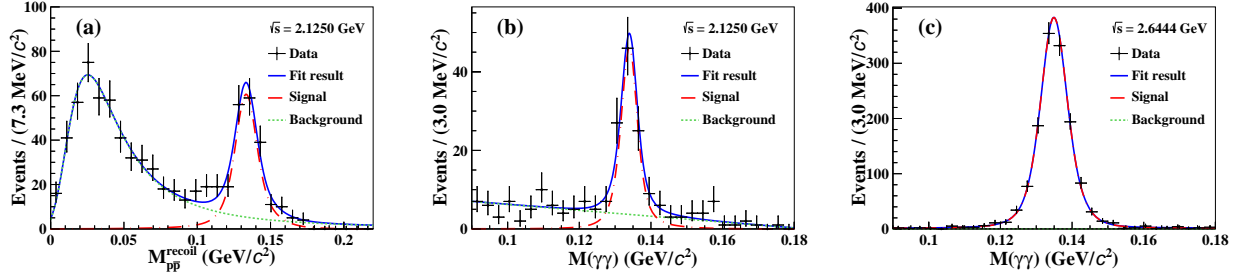


FIG. 1. Fits to the distributions of (a) M_{pp}^{recoil} in Mode I and (b) $M(\gamma\gamma)$ in Mode II at $\sqrt{s} = 2.1250$ GeV, as well as (c) $M(\gamma\gamma)$ at $\sqrt{s} = 2.6444$ GeV for full reconstruction. The black dots with error bars are data and the blue solid lines are the fit results. The red dash-dotted lines are the fitted signal shapes, while the green dashed lines are the fitted background shapes.

TABLE II. The measured Born cross sections for $e^+e^- \rightarrow p\bar{p}\pi^0$, where the first uncertainties are statistical and the second ones are systematic. At \sqrt{s} from 2.1000 to 2.2324 GeV, partial reconstruction is used. At \sqrt{s} from 2.3094 to 3.0800 GeV, full reconstruction is used and the Born cross sections have been corrected by $\mathcal{B}(\pi^0 \rightarrow \gamma\gamma)$.

\sqrt{s} (GeV)	\mathcal{L} (pb $^{-1}$)	N_{Signal}	ϵ (%)	$(1 + \delta)$	$\frac{1}{ 1 - \Pi ^2}$	σ^{B} (pb)
2.1000	12.2 ± 0.1	$7.9^{+4.3}_{-3.3}$	8.7	0.794	1.039	$9.0^{+4.9}_{-3.8} \pm 1.2$
2.1250	108 ± 1	294.7 ± 19.8	17.6	0.804	1.039	$18.6 \pm 1.2 \pm 0.8$
2.1500	2.84 ± 0.02	$23.2^{+5.7}_{-5.3}$	25.3	0.816	1.040	$38.1^{+9.4}_{-8.7} \pm 2.0$
2.1750	10.6 ± 0.1	100.9 ± 11.7	31.8	0.828	1.040	$34.8 \pm 4.0 \pm 2.1$
2.2000	13.7 ± 0.1	198.8 ± 15.3	32.6	0.845	1.040	$50.7 \pm 3.9 \pm 2.5$
2.2324	11.9 ± 0.1	202.5 ± 15.5	42.5	0.867	1.041	$44.4 \pm 3.4 \pm 2.3$
2.3094	21.1 ± 0.1	300.3 ± 17.9	23.5	0.876	1.041	$67.2 \pm 4.0 \pm 2.5$
2.3864	22.5 ± 0.2	568.3 ± 25.2	26.6	0.866	1.041	$106.5 \pm 4.7 \pm 3.9$
2.3960	66.9 ± 0.5	1824.7 ± 44.0	26.4	0.866	1.041	$115.9 \pm 2.8 \pm 4.2$
2.5000	1.10 ± 0.01	34.7 ± 6.0	29.8	0.899	1.041	$114.5 \pm 19.8 \pm 8.7$
2.6444	33.7 ± 0.2	1376.8 ± 38.6	31.5	0.958	1.039	$131.9 \pm 3.7 \pm 4.1$
2.6464	34.0 ± 0.3	1386.9 ± 38.0	31.7	0.958	1.039	$130.8 \pm 3.6 \pm 4.3$
2.7000	1.04 ± 0.01	39.0 ± 6.2	31.2	0.981	1.039	$119.2 \pm 19.0 \pm 3.6$
2.8000	1.01 ± 0.01	28.0 ± 5.3	33.8	1.022	1.037	$78.3 \pm 14.8 \pm 3.3$
2.9000	105 ± 1	2576.2 ± 52.5	33.6	1.063	1.033	$67.4 \pm 1.4 \pm 2.0$
2.9500	15.9 ± 0.1	318.0 ± 17.8	33.4	1.084	1.029	$54.3 \pm 3.0 \pm 1.8$
2.9810	16.1 ± 0.1	330.0 ± 18.2	33.7	1.096	1.025	$54.8 \pm 3.0 \pm 1.6$
3.0000	15.9 ± 0.1	290.3 ± 17.6	33.7	1.103	1.021	$48.7 \pm 3.0 \pm 1.6$
3.0200	17.3 ± 0.1	321.0 ± 17.9	34.2	1.115	1.014	$48.6 \pm 2.7 \pm 1.4$
3.0800	126 ± 1	1832.4 ± 43.7	31.4	1.178	0.915	$43.4 \pm 1.0 \pm 1.3$

The uncertainty from the ISR and VP correction factors is assigned to be 0.5% according to the accuracy of the radiation function [29]. The additional contribution from the cross section line shape is evaluated by varying the parameters of the fitting model. All parameters are randomly varied within their uncertainties and the resulting parametrization of the line shape is used to recalculate $(1 + \delta)$, ϵ and the corresponding cross sections. This procedure is repeated 1000 times and the standard deviation of the resulting cross sections is taken as the systematic uncertainty.

The uncertainties related to the fit procedure are estimated by changing the fit range, replacing the signal shape with a Breit-Wigner convolved with a Gaussian function, and replacing the background shape with a second-order polynomial function except in Mode I whose background shape is changed to the MC-simulated shape from the exclusive process $e^+e^- \rightarrow p\bar{p}$. This MC sample of $e^+e^- \rightarrow p\bar{p}$ is generated by PHOKHARA [22] with both ISR and final state radiation enabled. The uncertainties due to the background shape for full reconstruction are ne-

glected. The uncertainty arising from the signal MC model is evaluated using an alternative amplitude model, while the quoted mass and width are smeared with their associated uncertainties. The relative difference in the detection efficiency is taken as the uncertainty.

At \sqrt{s} from 2.1000 and 2.2324 GeV two partial reconstruction methods (Mode I and Mode II) are applied. The uncertainties of these two methods are weighted by detection efficiencies and averaged. The weighted average formula is

$$\sigma_{\text{tot}}^2 = \sum_{i=1}^2 \omega_i^2 \sigma_i^2 + \sum_{i,j=1;i \neq j}^2 \rho_{ij} \omega_i \omega_j \sigma_i \sigma_j, \quad (2)$$

with

$$\omega_i = \frac{\varepsilon_i}{\sum_{i=1}^2 \varepsilon_i}, \quad (3)$$

where ω_i , σ_i and ε_i with $i = 1, 2$ are the weight, systematic uncertainty and efficiency for reconstruction method i , respectively, and ρ_{ij} is the correlation parameter for the two

TABLE III. The selected components at each energy point except $\sqrt{s} = 2.1000, 2.1500$ and 2.1750 GeV. These three energy points use the fit results obtained by $\sqrt{s} = 2.1250$ GeV.

\sqrt{s} (GeV)	Components selected
2.1250, 2.2000, 2.2324	$N(940), \rho(1900)$
2.3094, 2.5000	$N(940), \Delta(1232), \rho(2000)$
2.3864	$\Delta(1232), \rho(2000)$
2.3960	$N(940), \Delta(1232), \rho(2000), \rho(2225)$
2.6444, 2.6464, 2.7000	$\Delta(1232), N(1520), N(1650), \rho(1900)$
2.8000	$N(940), \Delta(1232), \rho(2225)$
2.9000, 2.9500, 2.9810	$\Delta(1232), N(1440), N(1520), N(1710), \rho(2000), \rho(2225)$
3.0000, 3.0200, 3.0800	$\Delta(1232), \Delta(1600), N(1520), N(1710), N(1895)$

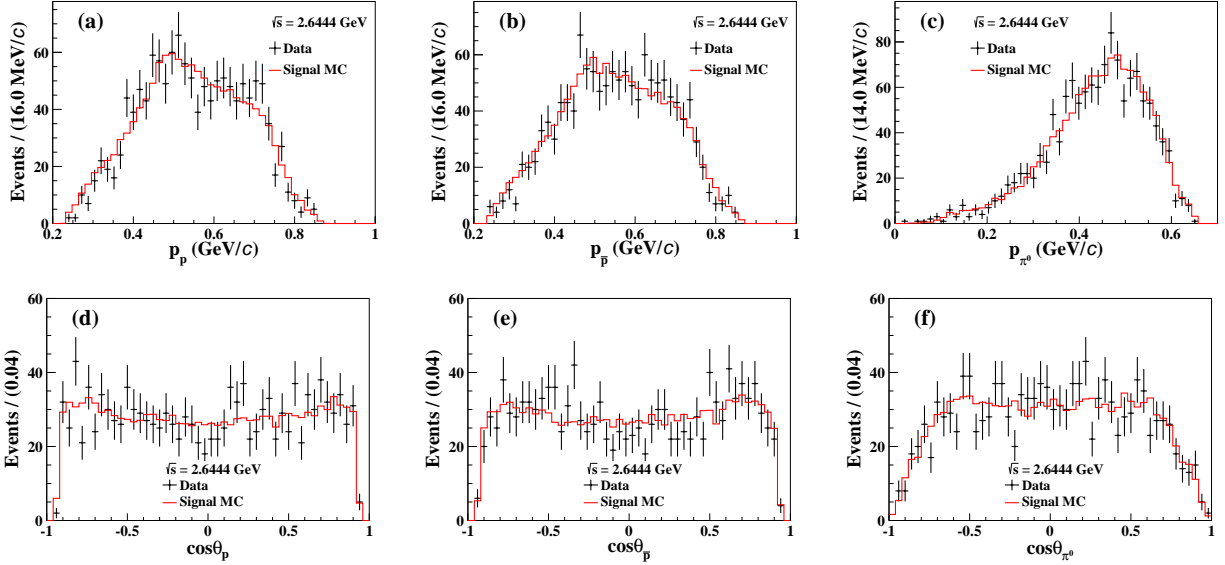


FIG. 2. The momentum distributions of (a) p , (b) \bar{p} and (c) π^0 and the angular distributions of (d) p , (e) \bar{p} and (f) π^0 at $\sqrt{s} = 2.6444$ GeV. The black dots with error bars are data and the red histograms are signal MC sample.

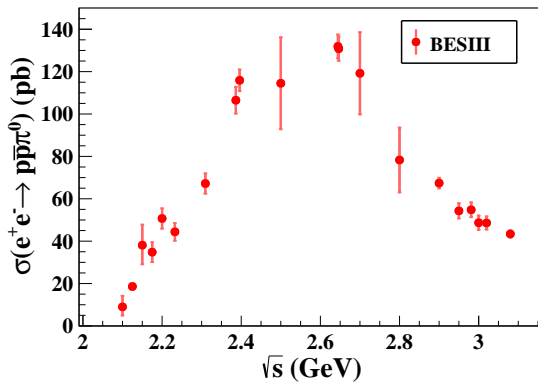


FIG. 3. The measured Born cross sections for the process $e^+e^- \rightarrow p\bar{p}\pi^0$.

different methods i and j . For the uncorrelated systematic uncertainties, like the uncertainties from the photon reconstruction efficiency, the requirements of $\theta_{\gamma\bar{p}} \geq 30^\circ$, $\theta_{p\bar{p}} \leq 173^\circ$ and $|\cos\theta_{\pi^0}| \leq 0.96$, the kinematic fit and fit

procedure, the ρ_{ij} values are set to be zero. For other correlated systematic uncertainties, like the uncertainties related to luminosity, tracking, PID, ISR and VP correction factors and the MC model, the ρ_{ij} are set to be one. After weighting, the systematic uncertainty of the kinematic fit is less than 0.1% and is neglected.

The combined results from different partial reconstruction methods are summarized in Table IV, while the systematic uncertainties related to full reconstruction are listed in Table V. The total systematic uncertainty is summed in quadrature.

VI. SUMMARY AND DISCUSSION

This paper presents the measurement of the Born cross sections for the process $e^+e^- \rightarrow p\bar{p}\pi^0$ at 20 c.m. energies, corresponding to a total integrated luminosity of 636.8 pb^{-1} , in the energy range from 2.1000 to 3.0800 GeV. The uncertainties at most energy points are less than 10%. The dominant contribution to the uncertainties is statistical near the energy threshold and systematic at higher energies. An increase around 2.4 GeV in the cross sec-

TABLE IV. Relative systematic uncertainties (in %) on the cross section measurement for each c.m. energy from 2.1000 to 2.2324 GeV. They are denoted as luminosity (\mathcal{L}), Tracking (Track), PID, photon reconstruction (Photon), requirements of $\theta_{\gamma\bar{p}} \geq 30^\circ$ ($\theta_{\gamma\bar{p}1}$), $\theta_{p\bar{p}} \leq 173^\circ$, and $|\cos\theta_{\pi^0}| \leq 0.96$, ISR correction, signal shape (Sig), background shape (Bkg), fit range (Fit) and signal MC model (MC). The last column is the total systematic uncertainty.

\sqrt{s} (GeV)	\mathcal{L}	Track	PID	Photon	$\theta_{\gamma\bar{p}1}$	$\theta_{p\bar{p}}$	$\cos\theta_{\pi^0}$	ISR correction	Sig	Bkg	Fit	MC	Total
2.1000	0.7	3.3	0.8	0.6	0.4	0.3	0.2	0.6	4.2	12.0	3.0	0.6	13.6
2.1250	0.8	3.4	0.8	0.4	0.3	0.3	0.3	0.6	1.3	1.2	0.4	1.1	4.2
2.1500	0.8	3.1	0.9	0.3	0.3	0.3	0.3	0.6	2.3	1.5	2.3	1.5	5.2
2.1750	0.8	2.9	0.9	0.3	0.2	0.3	0.3	0.6	4.6	0.3	1.8	1.6	6.1
2.2000	0.7	2.6	1.0	0.3	0.2	0.3	0.3	0.6	3.0	0.6	0.9	2.5	5.0
2.2324	0.7	2.3	1.0	0.2	0.2	0.3	0.3	0.9	2.9	1.2	0.4	2.8	5.1

TABLE V. Relative systematic uncertainties (in %) on the cross section measurement for each c.m. energy from 2.3094 to 3.0800 GeV. They are denoted as luminosity (\mathcal{L}), Tracking (Track), PID, requirement of $\theta_{\gamma\bar{p}} \geq 20^\circ$ ($\theta_{\gamma\bar{p}2}$), π^0 reconstruction, ISR correction, signal shape (Sig), fit range (Fit) and signal MC model (MC). The last column is the total systematic uncertainty.

\sqrt{s} (GeV)	\mathcal{L}	Track	PID	$\theta_{\gamma\bar{p}2}$	π^0 reconstruction	ISR correction	Sig	Fit	MC	Total
2.3094	0.7	1.9	1.1	0.6	2.5	0.5	0.9	0.3	0.8	3.7
2.3864	0.8	1.9	1.1	0.6	2.5	0.5	1.1	0.4	0.3	3.7
2.3960	0.7	1.8	1.1	0.6	2.5	0.5	0.2	0.3	1.1	3.6
2.5000	0.8	1.6	0.9	0.6	2.5	0.5	6.7	1.2	0.2	7.6
2.6444	0.6	1.3	0.8	0.6	2.5	0.5	0.3	0.1	0.1	3.1
2.6464	0.8	1.3	0.8	0.6	2.5	0.5	1.1	0.1	0.1	3.3
2.7000	0.7	1.1	0.7	0.6	2.5	0.5	0.0	0.6	0.1	3.1
2.8000	0.7	0.8	0.6	0.6	2.5	0.5	0.0	3.1	0.3	4.2
2.9000	0.9	0.8	0.6	0.6	2.5	0.5	0.2	0.2	0.1	2.9
2.9500	0.9	0.8	0.5	0.6	2.5	0.5	1.6	0.2	0.1	3.3
2.9810	0.6	0.8	0.5	0.6	2.5	0.5	0.8	0.4	0.2	3.0
3.0000	0.7	0.7	0.5	0.6	2.5	0.5	1.5	0.4	0.2	3.2
3.0200	0.7	0.7	0.5	0.6	2.5	0.5	0.2	0.3	0.4	2.9
3.0800	0.7	0.8	0.5	0.6	2.5	0.5	0.6	0.2	0.4	3.0

tions, which may be from the $pN(1440)$ threshold, requires further experimental studies. No obvious threshold enhancement is observed in the cross sections. Intermediate states are investigated utilizing the FDC-PWA package. Due to low statistics, extracting the N^* and Δ^* yields and measuring the cross sections of two-body processes is still challenging. An improved PWA of the process $e^+e^- \rightarrow p\bar{p}\pi^0$ is highly desirable in order to study the intermediate resonances such as N^* or Δ^* coupling to $p\pi^0$ and $\bar{p}\pi^0$ or 1^- vector states coupling to $p\bar{p}$. These improved analyses could be achieved with the much larger data sets expected at the forthcoming advanced super tau-charm facilities [30, 31].

ACKNOWLEDGMENTS

The BESIII Collaboration thanks the staff of BEPCII, the IHEP computing center and the supercomputing center of the University of Science and Technology of China (USTC) for their strong support. This work is supported in part by National Key R&D Program of China under Contracts Nos. 2020YFA0406400, 2020YFA0406300, 2023YFA1606000, 2023YFA1609400; National Natural Science Foundation of China (NSFC) under Contracts Nos. 11625523, 11635010, 11735014, 11835012, 11935015, 11935016, 11935018, 11961141012,

12005219, 12025502, 12035009, 12035013, 12061131003, 12122509, 12105276, 12175244, 12192260, 12192261, 12192262, 12192263, 12192264, 12192265, 12221005, 12225509, 12235017; the Chinese Academy of Sciences (CAS) Large-Scale Scientific Facility Program; the CAS Center for Excellence in Particle Physics (CCEPP); Joint Large-Scale Scientific Facility Funds of the NSFC and CAS under Contract Nos. U1832207, U2032111, U1732263, U1832103; CAS Key Research Program of Frontier Sciences under Contracts Nos. QYZDJ-SSW-SLH003, QYZDJ-SSW-SLH040; CAS Youth Team Program under Contract No. YSBR-101; 100 Talents Program of CAS; The Institute of Nuclear and Particle Physics (INPAC) and Shanghai Key Laboratory for Particle Physics and Cosmology; European Union's Horizon 2020 research and innovation programme under Marie Skłodowska-Curie grant agreement under Contract No. 894790; German Research Foundation DFG under Contracts Nos. 455635585, Collaborative Research Center CRC 1044, FOR5327, GRK 2149; Istituto Nazionale di Fisica Nucleare, Italy; Ministry of Development of Turkey under Contract No. DPT2006K-120470; National Research Foundation of Korea under Contract No. NRF-2022R1A2C1092335; National Science and Technology fund of Mongolia; National Science Research and Innovation Fund (NSRF) via the Program Management Unit for Human Resources & Institutional Development, Research and Innovation of Thailand under

Contract No. B16F640076; Polish National Science Centre under Contract No. 2019/35/O/ST2/02907; The

Swedish Research Council; U. S. Department of Energy under Contract No. DE-FG02-05ER41374.

-
- [1] M. Ablikim *et al.* (BESIII Collaboration), *Phys. Rev. D* **91**, 112004 (2015).
- [2] M. Ablikim *et al.* (BESIII Collaboration), *Phys. Rev. Lett.* **124**, 042001 (2020).
- [3] M. Ablikim *et al.* (BESIII Collaboration), *Phys. Rev. D* **99**, 092002 (2019).
- [4] M. Ablikim *et al.* (BESIII Collaboration), *Phys. Lett. B* **817**, 136328 (2021).
- [5] L. Xia, C. Rosner, Y. D. Wang, X. Zhou, F. E. Maas, R. B. Ferroli, H. Hu, and G. Huang, *Symmetry* **14**, 231 (2022).
- [6] M. Ablikim *et al.* (BESIII Collaboration), *Phys. Rev. Lett.* **120**, 132001 (2018).
- [7] M. Ablikim *et al.* (BESIII Collaboration), *Phys. Rev. Lett.* **131**, 191901 (2023).
- [8] M. Ablikim *et al.* (BESIII Collaboration), *Phys. Rev. D* **97**, 032013 (2018).
- [9] M. Ablikim *et al.* (BESIII Collaboration), *Phys. Rev. D* **107**, 072005 (2023).
- [10] G. Huang and R. B. Ferroli, *Natl. Sci. Rev.* **8**, nwab187 (2021).
- [11] M. Ablikim *et al.* (BESIII Collaboration), *Phys. Rev. D* **109**, 012002 (2024).
- [12] M. Ablikim *et al.* (BESIII Collaboration), *Phys. Rev. D* **90**, 032007 (2014).
- [13] M. Ablikim *et al.* (BESIII Collaboration), *Phys. Lett. B* **771**, 45 (2017).
- [14] G. I. Gakh, A. P. Rekalov, E. Tomasi-Gustafsson, J. Boucher, and A. G. Gakh, *Phys. Rev. C* **83**, 025202 (2011).
- [15] M. F. M. Lutz *et al.* (PANDA Collaboration), [arXiv:0903.3905](https://arxiv.org/abs/0903.3905).
- [16] M. Ablikim *et al.* (BESIII Collaboration), *Nucl. Instrum. Meth. A* **614**, 345 (2010).
- [17] Y. F. Wang, *Int. J. Mod. Phys. A* **21**, 5371 (2006).
- [18] K. X. Huang *et al.*, *Nucl. Sci. Tech.* **33**, 142 (2022).
- [19] S. Agostinelli *et al.* (GEANT4 Collaboration), *Nucl. Instrum. Meth. A* **506**, 250 (2003).
- [20] R. G. Ping, *Chin. Phys. C* **38**, 083001 (2014).
- [21] J.-X. Wang, *Nucl. Instrum. Meth. A* **534**, 241 (2004).
- [22] H. Czyż, P. Kiszka, and S. Tracz, *EPJ Web Conf.* **142**, 01010 (2017).
- [23] B. Andersson and H. M. Hu, [arXiv:hep-ph/9910285](https://arxiv.org/abs/hep-ph/9910285).
- [24] K. S. Kolbig and B. Schorr, *Comput. Phys. Commun.* **31**, 97 (1984), [Erratum: *Comput. Phys. Commun.* 178, 972 (2008)].
- [25] R. L. Workman *et al.* (Particle Data Group), *PTEP* **2022**, 083C01 (2022).
- [26] W. Y. Sun, T. Liu, M. Q. Jing, L. L. Wang, B. Zhong, and W. M. Song, *Front. Phys. (Beijing)* **16**, 64501 (2021).
- [27] M. Ablikim *et al.* (BESIII Collaboration), *Chin. Phys. C* **41**, 113001 (2017).
- [28] M. Ablikim *et al.* (BESIII Collaboration), *Phys. Rev. D* **99**, 011101 (2019).
- [29] S. Actis *et al.* (Working Group on Radiative Corrections, Monte Carlo Generators for Low Energies), *Eur. Phys. J. C* **66**, 585 (2010).
- [30] M. Achasov *et al.*, *Front. Phys. (Beijing)* **19**, 14701 (2024).
- [31] D. A. Epifanov (SCTF Collaboration), *Phys. Atom. Nucl.* **83**, 944 (2020).